

This is a repository copy of *Unexpected Formation of Organic Siloxanes alongside Ethylphenols in the Catalytic Hydrogenation of Waste Enzymatic Lignin*.

White Rose Research Online URL for this paper:

<https://eprints.whiterose.ac.uk/id/eprint/175969/>

Version: Published Version

---

**Article:**

Feng, Shanshan, Liu, Xudong, Fan, Jiajun orcid.org/0000-0003-3721-5745 et al. (2 more authors) (2021) Unexpected Formation of Organic Siloxanes alongside Ethylphenols in the Catalytic Hydrogenation of Waste Enzymatic Lignin. *Advanced Energy and Sustainability Research*. 2100059. ISSN: 2699-9412

<https://doi.org/10.1002/aesr.202100059>

---

**Reuse**

This article is distributed under the terms of the Creative Commons Attribution (CC BY) licence. This licence allows you to distribute, remix, tweak, and build upon the work, even commercially, as long as you credit the authors for the original work. More information and the full terms of the licence here:

<https://creativecommons.org/licenses/>

**Takedown**

If you consider content in White Rose Research Online to be in breach of UK law, please notify us by emailing [eprints@whiterose.ac.uk](mailto:eprints@whiterose.ac.uk) including the URL of the record and the reason for the withdrawal request.

# Unexpected Formation of Organic Siloxanes alongside Ethylphenols in the Catalytic Hydrogenation of Waste Enzymatic Lignin

Shanshan Feng, Xudong Liu, Jiajun Fan, Changwei Hu,\* and James H. Clark\*

A multifunctional Ru/SBA-15 catalyst is prepared via impregnation and used in the depolymerization of crude waste corn stover enzymatic lignin (CSEL) to produce monophenols and, unexpectedly, the industrially important organic siloxanes. In the depolymerization of CSEL over Ru/SBA-15, a high phenolic monomer yield of 13.91 wt% with a high selectivity to ethylphenols ( $\approx 61\%$ ) can be achieved. Unexpectedly, when the reaction is carried out in ethanol, the predictable phenolic products are accompanied by both diethyl dimethyl orthosilicate and tetraethyl orthosilicate with the methyl group likely to come from lignin methoxy groups. Changing to a different alcohol solvent changes the siloxane products accordingly. The characterization of catalysts indicates that Ru<sup>0</sup> is the active species in Ru/SBA-15 catalysts and is well dispersed with small particle size (6.2 nm). This catalyst significantly contributes to both the production of phenols and siloxanes and contributes to the hydrogenolysis/hydrogenation of lignin.

20%–30% in weight among lignocellulosic biomass, is by far the most abundant renewable aromatic resource in nature. The high functionalization and aromatization of lignin make it a potential feedstock for producing value-added phenolic compounds.<sup>[2]</sup> However, due to the complexity and the heterogeneity of lignin structure, the conversion and utilization of lignin are confronted with great challenges and obstacles.<sup>[3]</sup> In addition, the monolignol units of lignin structures vary greatly in different biomass feedstocks (e.g., hardwood, softwood, and grass).<sup>[4]</sup>

Due to the less recalcitrance and more homogeneity of carbohydrates structure, great progress has been achieved in the deconstruction of carbohydrates to obtain various value-added chemicals.<sup>[5]</sup>

Consequently, the valorization of lignin has been poorly exploited, although there is now a “lignin first” movement that seeks to improve on that.<sup>[6]</sup> A large proportion of lignin is obtained as agro-industrial wastes and side products, including Kraft lignin (from pulping industry) and enzymatic hydrolysis lignin (from cellulosic ethanol industries).<sup>[7]</sup> It has been reported that 50 million tons of lignin wastes were generated in the world paper industry annually.<sup>[8]</sup> However, the failure to exploit the chemical potential of lignin has led to its direct combustion of the majority of lignin-derived wastes, which has aggravated the CO<sub>2</sub>-emission and green-house effect issues.<sup>[9]</sup> In addition, the principles of environmentally benign and economic viability as well as zero waste should be prioritized equally to develop a biorefinery protocol to valorize the high-value of lignin wastes.<sup>[10]</sup>


The intrinsic structure of protolignin is modified during the delignification process in the industry, especially in Kraft pulping.<sup>[11]</sup> Previous studies have shown the cracking of  $\beta$ -O-4 ether bonds and concomitant occurrence of highly condensed fragments during pulping, hindering subsequent efficient valorization.<sup>[12]</sup> In contrast, the pretreatment process in bio-ethanol production to obtain enzymatic hydrolysis lignin is relatively mild; hence, the structure of lignin has not been severely altered.<sup>[13]</sup> However, enzymatic hydrolysis lignin presents another problem—generally, it contains about 30 wt% of unreacted carbohydrates due to the enzyme inaccessibility to all parts of the biomass. In our previous work, we used the microwave-assisted conversion of the residual saccharides in crude waste softwood hydrolysis lignin (CSHL) to achieve an

## 1. Introduction

With diminishing reserves of fossil resources and increasing concerns over environmental issues, lignocellulosic biomass has attracted considerable attention as a renewable resource that can be converted into platform and specialty chemicals as well as high-quality fuels and materials.<sup>[1]</sup> Lignin, accounting for about

S. Feng, X. Liu, Prof. C. Hu  
Key Laboratory of Green Chemistry and Technology  
Ministry of Education  
College of Chemistry  
Sichuan University  
Chengdu 610064, China  
E-mail: changwei.hu@scu.edu.cn

Dr. J. Fan, Prof. J. H. Clark  
Green Chemistry Centre of Excellence  
Department of Chemistry  
University of York  
Heslington, York YO10 5DD, UK  
E-mail: james.clark@york.ac.uk

 The ORCID identification number(s) for the author(s) of this article can be found under <https://doi.org/10.1002/aesr.202100059>.

© 2021 The Authors. Advanced Energy and Sustainability Research published by Wiley-VCH GmbH. This is an open access article under the terms of the Creative Commons Attribution License, which permits use, distribution and reproduction in any medium, provided the original work is properly cited.

DOI: 10.1002/aesr.202100059

8 wt% yield of the industrially important levoglucosenone (LGO; a precursor to the new industrial bio-based solvent Cyrene) based on lignin, which equals to a 40% yield based on the residual saccharides.<sup>[14]</sup>

In fact, many “real” industrial lignins contain significant quantities of other contaminants notably silicates. These have been essentially ignored in previous studies on lignin or are not relevant, as so much of this research has focused on model compounds or purified materials rather than “real world” sample. Alkoxysilanes have many industrial applications, including in coating, for anti-corrosion, in catalyst preparation, and as coupling agents,<sup>[15]</sup> and their production normally involves working with toxic  $\text{SiCl}_4$  (and leading to the generation of large volumes of HCl). Their production from industrial waste as well as LGO and alongside phenolics both show the complexity of working with industrial lignins and the diverse value streams that can be created.

In this work, we have focused on the increasingly large industrial waste stream crude waste enzymatic hydrolysis lignin from corn stover (denoted as corn stover enzymatic lignin [CSEL]) and use it to demonstrate a method of capitalizing on the silicate contaminants while, at the same time, maximizing the yields of useful phenolic compounds.

## 2. Results and Discussion

### 2.1. Monophenols Obtained in Depolymerization of CSEL over Ru/SBA-15

The monophenols obtained in CSEL depolymerization are shown in Table S1, Supporting Information. They can be divided into p-hydroxyphenyl (H), guaiacol (G), and syringol (S) groups. It is observed that phenols (H, G, and S), 4-ethyl phenols (EH, EG, and ES), 4-vinyl phenols (VH and VG), p-coumaric acid (pCA), and ferulic acid (FA) are the major products.

#### 2.1.1. Effect of Depolymerization Temperature

The yields of the main monophenols for the depolymerization of CSEL under different conditions are shown in Figure 1. The effect of reaction temperature with and without catalyst in ethanol is shown in Figure 1a. It seems that temperature has a very important effect on the depolymerization of CSEL. When ethanol (EtOH) is used as solvent and in the absence of the catalyst, a low phenolic monomer yield of 3.30 wt% is obtained at 220 °C for 4 h, with vinylphenols (VH and VG) as the major products with a selectivity of 43.2% (Table S2, Supporting Information). These

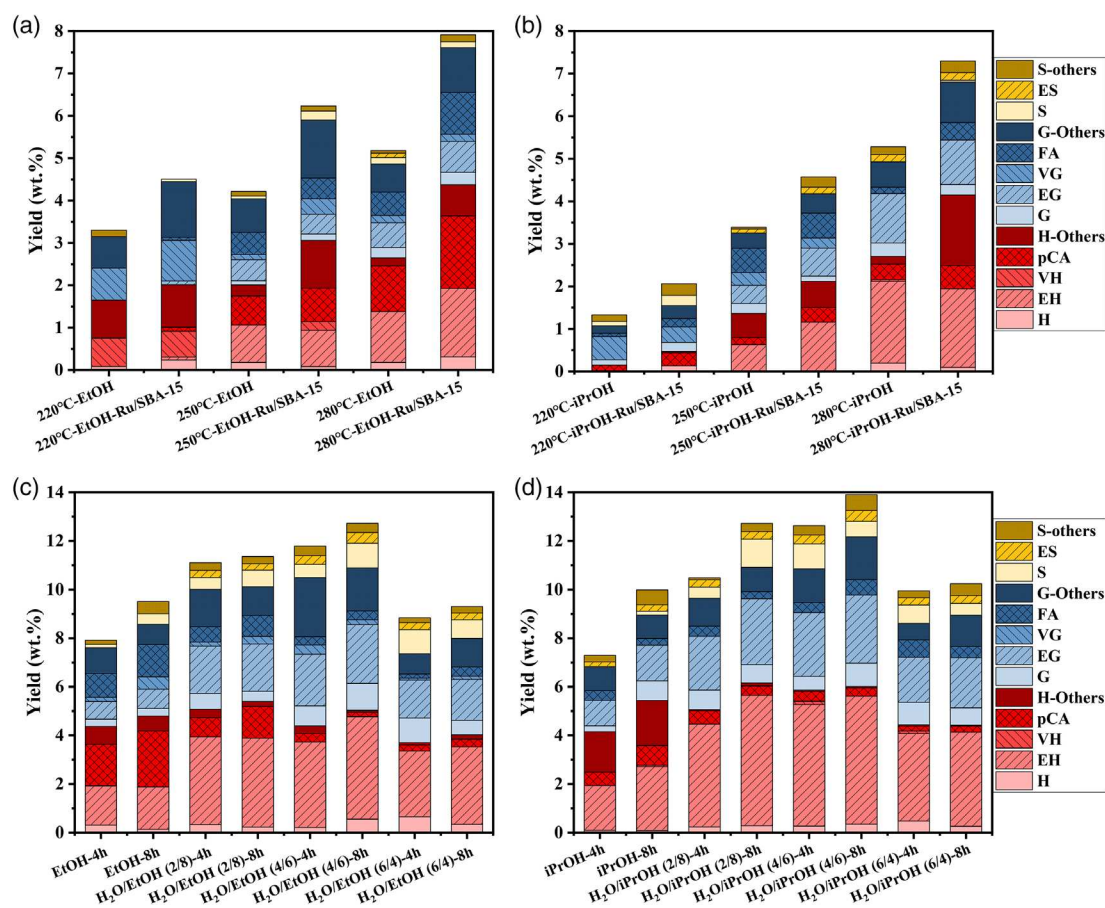


**Figure 1.** The yield and selectivity of monophenols as a function of temperature with a) ethanol and b) isopropanol as solvents (CSEL (0.5 g), solvent (50 mL), Ru/SBA-15 (0.2 g), 2 MPa  $\text{H}_2$ , 4 h). The yield and selectivity of monophenols in function of different solvent ratios with c)  $\text{H}_2\text{O}$ /ethanol and d)  $\text{H}_2\text{O}$ /isopropanol at 280 °C (CSEL (0.5 g), solvent (50 mL), Ru/SBA-15 (0.2 g), 2 MPa  $\text{H}_2$ ). The yield was calculated based on the lignin in CSEL (62.6%).

can be derived from the main structure units of pCA and FA in grass lignin.<sup>[16]</sup> In the presence of Ru/SBA-15 catalyst, the phenolic monomer yield increases slightly to 4.50 wt%, but the selectivity to vinylphenols decreases to 34.7% because of the formation of ethylphenols (mainly EH and EG). When the temperature is higher than 250 °C, the product distribution shifts to ethylphenols, and the selectivity to vinyl substituted products decreases with increasing temperature. FA and pCA can also be detected as the major products, which indicates that temperature is very important for the breaking of C—O—C bond and the selective hydrogenation of —C=C— side chain in CSEL-derived intermediates. The variation in the distribution of the products in the presence of Ru/SBA-15 is almost the same as that without catalyst, with increased monophenols yields (7.91 wt%) at 280 °C. The results using isopropanol (iPrOH) as solvent are shown in Figure 1b, and the specific yields and selectivity are shown in Table S3, Supporting Information. It can be seen that the effect of temperature on the depolymerization of CSEL is more obvious compared with using ethanol as solvent: the monomer yield increased from 1.65 wt% at 220 °C to 5.28 wt% at 280 °C in the absence of Ru/SBA-15, and from 2.23 to 7.30 wt% in the presence of Ru/SBA-15. It is noticed that the yields of monophenols obtained in ethanol solvent are slightly higher than those obtained in isopropanol both in the absence and presence of Ru/SBA-15.

### 2.1.2. Effect of Solvent Ratio and Time

The solvent ratio can also influence the depolymerization of CSEL and the distribution of monophenols. Figure 1c,d shows the yield and distribution of monophenols in H<sub>2</sub>O/ethanol and H<sub>2</sub>O/isopropanol cosolvent systems in the presence of Ru/SBA-15, and the specific yields are shown in Table S4 and S5, Supporting Information. When the ratio of water/alcohol is 4/6, the yield of monophenols reaches the highest in both H<sub>2</sub>O/ethanol and H<sub>2</sub>O/isopropanol cosolvent system (12.72 and 13.91 wt% at 280 °C for 8 h, respectively). It is indicated in the presence of water; the yields of monophenols increase remarkably, and slightly higher yields are obtained in H<sub>2</sub>O/isopropanol cosolvent.

In pure ethanol solvent at 280 °C for 4 h, the selectivity to pCA and FA is 34.0%, and the selectivity to ethylphenols is 29.6%, whereas extending the reaction time to 8 h leads to increasing selectivity to pCA and FA (38.1%) with the selectivity to ethylphenols being 26.5%. In cosolvent systems, when the ratio of water to ethanol is increased from 2/8 to 6/4, the selectivity to all ethylphenols increases to over 50%. Prolonging the time from 4 to 8 h leads to increased yields of monophenols with each cosolvent ratio; however, the selectivity to pCA and FA is unchanged. We can, therefore, say that the increase of ethyl substituted phenols originates from the direct depolymerization of lignin, or parts of the pCA and FA newly produced are quickly converted to EH and EG under the reaction conditions. In a H<sub>2</sub>O/isopropanol system, the selectivity toward ethylphenols increases from about 40% in pure isopropanol to over 60% in H<sub>2</sub>O/isopropanol cosolvent, which is a little higher than that in H<sub>2</sub>O/ethanol cosolvent, and the selectivity to pCA and FA is both

maintained at 10 (±3)%. The variation trends of other products are almost the same as those in H<sub>2</sub>O/ethanol.

In the previous literature reports, cosolvent systems usually exhibit better lignocellulose dissolution than single solvent systems. Renders et al. studied the synergetic effects of H<sub>2</sub>O/alcohol on the catalytic reductive fractionation of poplar and found that low water concentrations (<30 vol%) enhanced the removal of lignin from the biomass, whereas high water (≥70 vol%) concentrations favored the solubilization of both hemicellulose and lignin.<sup>[17]</sup> In our previous work, an optimal solvent ratio of H<sub>2</sub>O/ethanol (v/v, 6/4) in the depolymerization of lignin in pubescens was observed, when the ratio of H<sub>2</sub>O/methanol was 3/7, and the highest yield of monophenols could be obtained from birch lignin.<sup>[18]</sup> Compared with pure alcohol solvents, H<sub>2</sub>O/alcohol cosolvent allows reactions under relatively mild conditions, as the cosolvent system offers both an electron acceptor solvent with high polarity (H<sub>2</sub>O) and an electron donor solvent with middle polarity (alcohol). Alcohol plays an important role in promoting the lignin hydrolysis and dissolving the depolymerized products. Furthermore, carboxylic acid formed in the lignin depolymerization could be esterified with alcohol, which inhibits the repolymerization of monomers to form biochar.<sup>[19]</sup> Bai et al. reported the depolymerization of lignin-rich corn cob residue (LRCR) in supercritical ethanol at 320 °C for 7.5 h with a yield of 147.9 mg g<sup>-1</sup> (14.79 wt%) for alkylphenol.<sup>[20]</sup> Jiang et al. used isopropanol as solvent and an in situ hydrogen source for the depolymerization of cellulosytic enzyme corn stover lignin and got a highest total monophenols yield of 8.14 wt% over Ni<sub>50</sub>Pd<sub>50</sub>/SBA-15. The yield of phenolic monomers was quite limited though bimetallic supported catalysts were applied.<sup>[21]</sup> In this work, the monophenols yield increases from 7.91 wt% in pure ethanol to 12.72 wt% in H<sub>2</sub>O/ethanol (v/v, 4/6) and 7.30 wt% in pure isopropanol to 13.91 wt% in H<sub>2</sub>O/isopropanol (v/v, 4/6), respectively. From the product distributions, it is found that the presence of water could also influence the distribution of monophenols depolymerized from CSEL, which effectively improves the formation of ethylphenols. Water might promote both the direct depolymerization of lignin and the further deacidification of pCA and FA to obtain vinylphenols, subsequently hydrogenated to ethyl phenols.

### 2.2. Siloxane Obtained in Pure Alcohol as Solvent

In pure ethanol solvent, gas chromatography (GC) and GC-mass spectrometry (MS) showed strong peaks that can be assigned to tetraethyl orthosilicate (TEOS) and diethyl dimethyl orthosilicate (EMOS) (Figure S1, Supporting Information). Pure samples were used to confirm the assignments (Figure S2, Supporting Information). A singlet in the aliphatic oxygenated side chain region of 2D heteronuclear single quantum coherence nuclear magnetic resonance (2D HSQC NMR) is evident at δC/δH 56.4/3.44 ppm and was significantly stronger with reaction to 8 h in ethanol solvent at 280 °C compared to that with reaction of 1 and 4 h (Figure 5). We believe that this can be assigned to the SiOCH<sub>2</sub>, for there are no singlet attributed to lignin structural nor monophenols appearing at δC/δH 56.4/3.44 ppm.<sup>[22]</sup> Furthermore, the singlet could not be detected in the NMR spectra of the liquid products obtained in the H<sub>2</sub>O/ethanol cosolvent



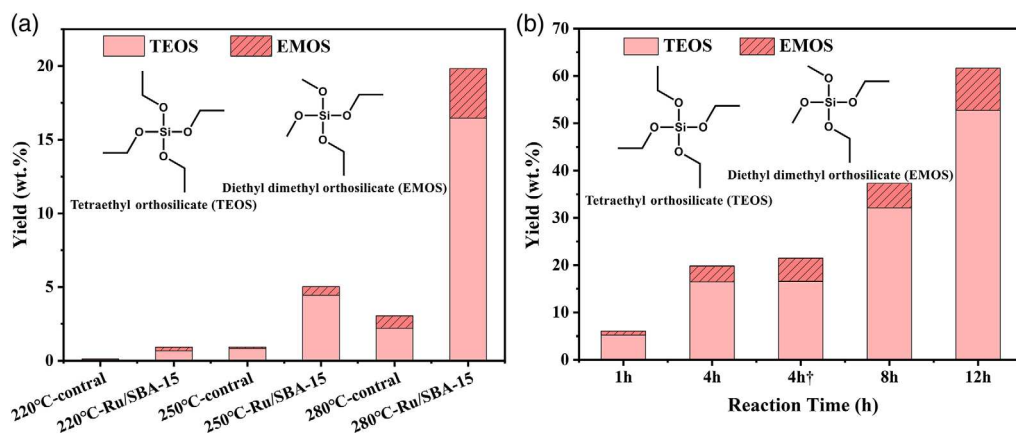


**Figure 2.** The effect of a) reaction temperature and b) reaction time on the yield of siloxanes. Reaction conditions: CSEL (0.5 g), ethanol (50 mL), Ru/SBA-15 (0.2 g), 280 °C, and 2 MPa H<sub>2</sub> (control reaction: CSEL (0.5 g), ethanol (50 mL), 280 °C, 2 MPa H<sub>2</sub>, and 4 h; 4 h†: CSEL (1.0 g), ethanol (50 mL), Ru/SBA-15 (0.2 g), 280 °C, 2 MPa H<sub>2</sub>, and 4 h).

system (Figure S3, Supporting Information). Products from the depolymerization of CSEL lignin were detected and recorded by quadrupole time-of-flight mass spectrometer (QTOF MS) within the  $m/z$  range of 100–500, where the peaks at 209.1213 and 231.1025 are assigned to the [TEOS + H]<sup>+</sup> and [TEOS + Na]<sup>+</sup>, respectively, and the peaks at 181.0901 and 203.0718 are assigned to the [TMOS + H]<sup>+</sup> and [TMOS + Na]<sup>+</sup>, respectively

(Figure S4, Supporting Information). With pure methanol as solvent, only tetramethyl orthosilicate (TMOS) was obtained. The blank experiment without CSEL and the control experiment using SiO<sub>2</sub> as starting material with Ru/SBA-15 and ethanol under the same conditions did not produce any siloxane-derived products, which suggests that the siloxanes cannot be derived from SBA-15 or SiO<sub>2</sub>. These facts confirm the formation of

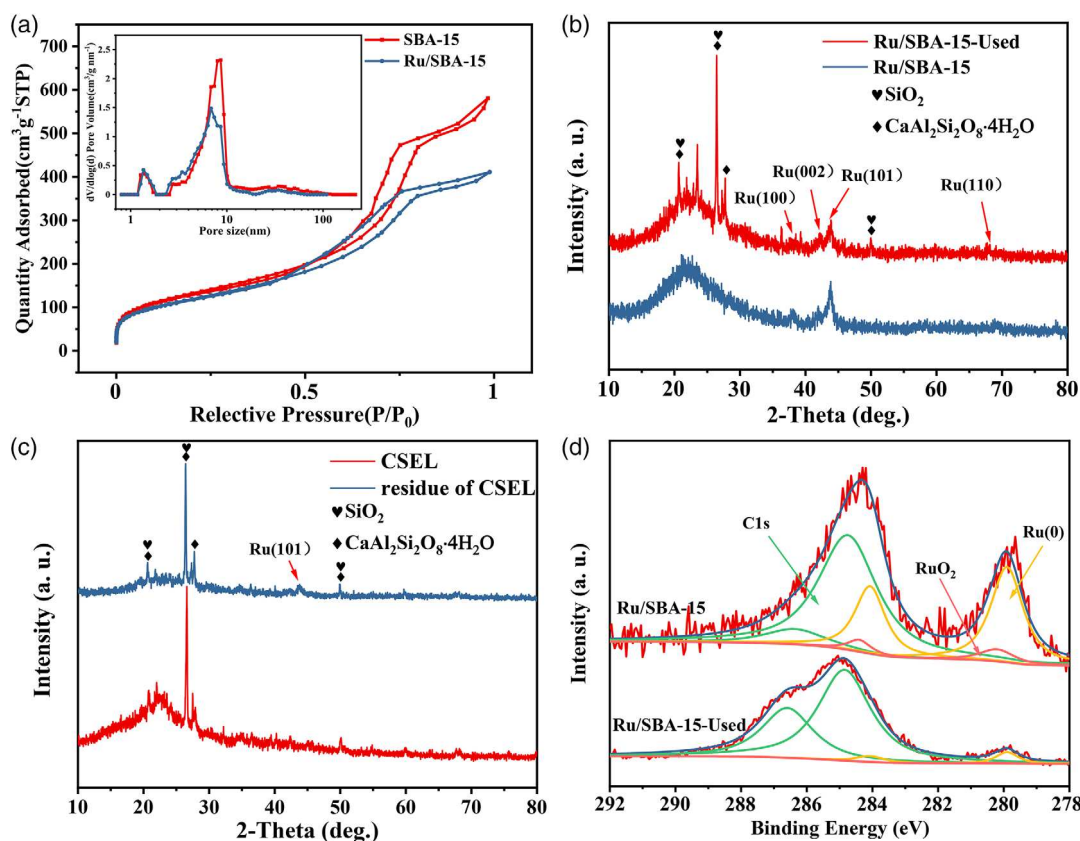


**Figure 3.** a) N<sub>2</sub> absorption–desorption isotherms and pore size distribution of Ru/SBA-15. b,c) XRD patterns of Ru/SBA-15 and CSEL before and after used in ethanol at 280 °C. d) XPS spectra of Ru 3d before and after used in ethanol at 280 °C.

TEOS and EMOS in the depolymerization process of enzymatic lignin, and the silicon comes from CSEL presumably, as the silicates known to be present in many types of biomass.<sup>[23]</sup>

Figure 2a shows the yield of siloxanes on reaction for 4 h at different temperatures. It can be observed that the presence of Ru/SBA-15 significantly increases the yield of siloxanes; most notably, the yield of siloxanes reached 19.83 wt% (based on the amount of Si in CSEL) in the presence of catalyst at 280 °C, which is about six times higher than that in the absence of catalyst (3.05 wt%). Figure 2b shows the yield of siloxanes as a function of reaction time at 280 °C, and the yield of siloxanes increases slightly to 21.47 wt% (Figure 2b, 4h†) by doubling the amount of CSEL. The highest yield of the siloxane of 61.63 wt% is obtained by prolonging the reaction time to 12 h.

When methanol is used as solvent, a large amount of TMOS is obtained with a yield of 43.26 wt% over Ru/SBA-15 at 280 °C for 4 h. This is significantly higher than the yield of TEOS (16.45 wt%) obtained under the same conditions. In the control reactions using methanol and ethanol (v/v, 2/8) as cosolvent, EMOS (9.76 wt%), triethyl methyl orthosilicate (TEMOS; 13.76 wt%), and TEOS (9.31 wt%) are obtained. This might be explained by the advantage of the smaller size of the methoxy group for the S<sub>N</sub>I substitution reaction. When pure isopropanol is used as the solvent, a small amount of tetraisopropyl orthosilicate (TIPOS) is also detected with a yield of 5.62 wt%, and this lower

yield might also be explained by the relative size of the alcohols. Furthermore, it should be noted that the siloxanes can only be obtained with alcohol solvent. No siloxane-derived products could be detected in H<sub>2</sub>O/alcohol cosolvent; presumably siloxanes would be hydrolyzed in water.

The formation of EMOS in reactions with ethanol as solvent is noteworthy. The Ru/SBA-15 might catalyze the cleavage of –OCH<sub>3</sub> in G or S unit to form methanol, or the formation of EMOS promoted the fracture of methoxy group. The hydrogenolysis of methoxy groups in G and S units has also been reported in Wang's work, where Pt/NiAl<sub>2</sub>O<sub>4</sub> promoted the cleavage of methoxy group to produce methanol, which then underwent aqueous methanol reforming affording H<sub>2</sub>.<sup>[24]</sup> In fact, according to the proportion of H-, G-, and S-type phenols in the reaction products (Table S6, Supporting Information), the proportion of H-type monophenols in pure ethanol solvent (≈50%) is significantly higher than that in water/ethanol mixed solvent (≈40%), which seems to confirm the cleavage of the methoxy group.

## 2.3. Characterizations

### 2.3.1. Catalyst Characterization

SBA-15 is used as the support for Ru/SBA-15 catalysts. Figure 3a shows the N<sub>2</sub> adsorption–desorption isotherms and pore size

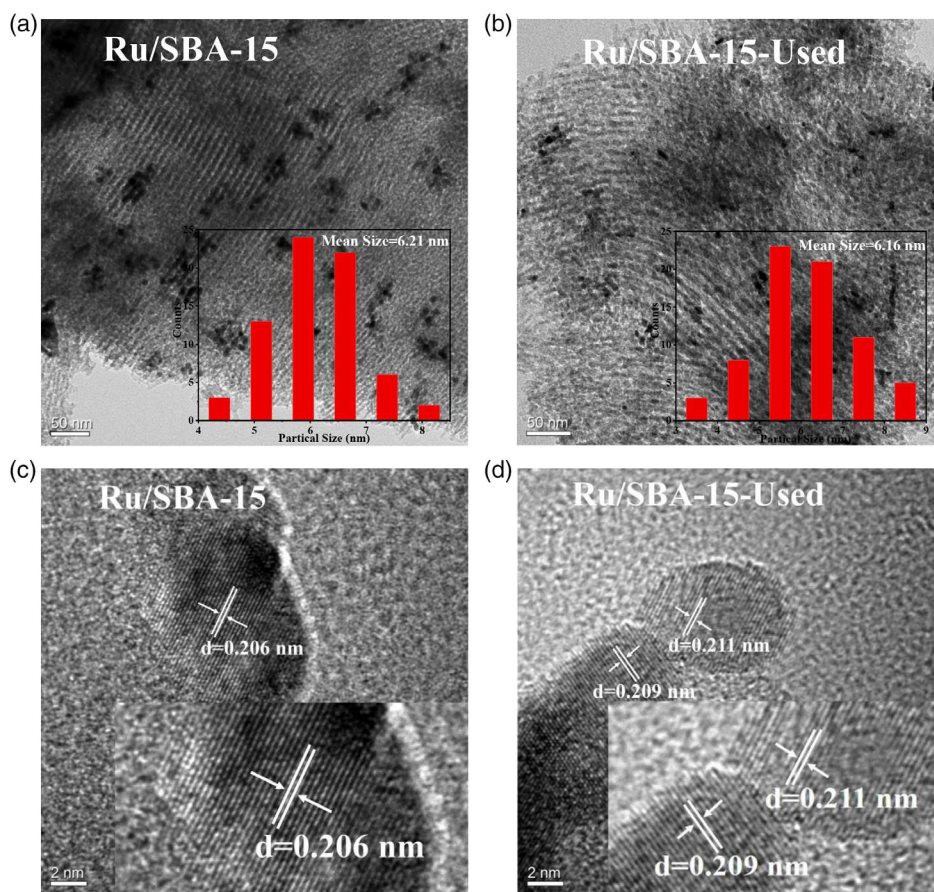


**Figure 4.** TEM images of a) Ru/SBA-15 and b) Ru/SBA-15 used in ethanol at 280 °C. HRTEM image of c) Ru/SBA-15 and d) Ru/SBA-15 used in ethanol at 280 °C.

distribution of SBA-15 and Ru/SBA-15. The surface area, pore volume, and pore width parameters are summarized in Table S7, Supporting Information. The pore width of the catalyst ranges from 5 to 9 nm; meanwhile, the isotherms show a representative IV-type isotherm with the hysteresis loops of typical H1-type, speculating a uniform pipe diameter material with open ends, and it could be confirmed in transmission electron microscopy (TEM) images. Figure 3b shows the X-ray diffraction (XRD) patterns of the Ru/SBA-15; it is shown that the carrier is amorphous, and the diffraction peaks at  $2\theta = 38.4^\circ$ ,  $42.1^\circ$ ,  $44.0^\circ$ , and  $69.4^\circ$  in the XRD pattern could be corresponding to Ru (100), (002), (101), and (110) (PDF#06-0663).<sup>[25]</sup> Before and after use of the catalyst, the most intense peak vest in  $\text{Ru}^0$  is Ru (101), which represents the hexagonal close packed of Ru species.

The X-ray photoelectron spectroscopy (XPS) of the Ru 3d is shown in Figure 3d, where two prominent peaks exhibit at 284.8 and 286.4 eV, which are assigned to C1s. The peaks observed at 279.9 eV ( $\text{Ru}^0 3d_{5/2}$ ) and 284.1 eV ( $\text{Ru}^0 3d_{3/2}$ ) indicate the presence of reduced state of Ru species, and the two small peaks observed at 280.2 eV ( $\text{Ru}^{6+} 3d_{5/2}$ ) and 284.4 eV ( $\text{Ru}^{6+} 3d_{3/2}$ ) imply the presence of  $\text{RuO}_2$ .<sup>[25b,26]</sup> The binding energies along with a quantitative estimation of the surface elements are given in Table S8, Supporting Information. Compared with the catalysts before use, the peaks of C1s are all enhanced after the reaction, probably because the catalyst is not completely separated from the reaction residue or some carbon deposited on the

surface of the catalyst. However,  $\text{Ru}^0$  keeps the main form of Ru on the surface; it is speculated that  $\text{Ru}^0$  is the active phase of the catalyst, and  $\text{RuO}_2$  may be oxidized instantly when taken out of the reduction furnace, but it can play a role of stabilizing the catalyst.<sup>[27]</sup>

The TEM images of Ru/SBA-15 are shown in Figure 4. It is shown that the SBA-15 carrier presents a tiled tubular arrangement, which substantiates the conjecture of Brunauer–Emmett–Teller (BET) isotherms. Ru particles could be observed with clear edges with the mean size of about 6.2 nm. Figure 4b shows the TEM images of Ru/SBA-15 used in the depolymerization of CSEL at  $280^\circ\text{C}$  in ethanol. It can be seen that the Ru particles agglomerate slightly at  $280^\circ\text{C}$  with the mean size rising to 8.29 nm, and the SBA-15 carrier maintains the original structure in ethanol. Figure 4c,d shows the high-resolution TEM (HRTEM) image of Ru/SBA-15, and the lattice spacing of 0.206, 0.209, and 0.211 nm is coincided with the Ru (101) and Ru (002) planes with the theoretical values of 0.205 and 0.214 nm, respectively, which agrees well with the XRD patterns.<sup>[18b,28]</sup>

### 2.3.2. Characterization of CSEL and the Liquid Products

**Structural Characterization of CSEL:** The XRD patterns of CSEL and the residue of CSEL reacted over Ru/SBA-15 in ethanol are shown in Figure 3c, where the most intense peaks at  $2\theta = 20.8^\circ$ ,

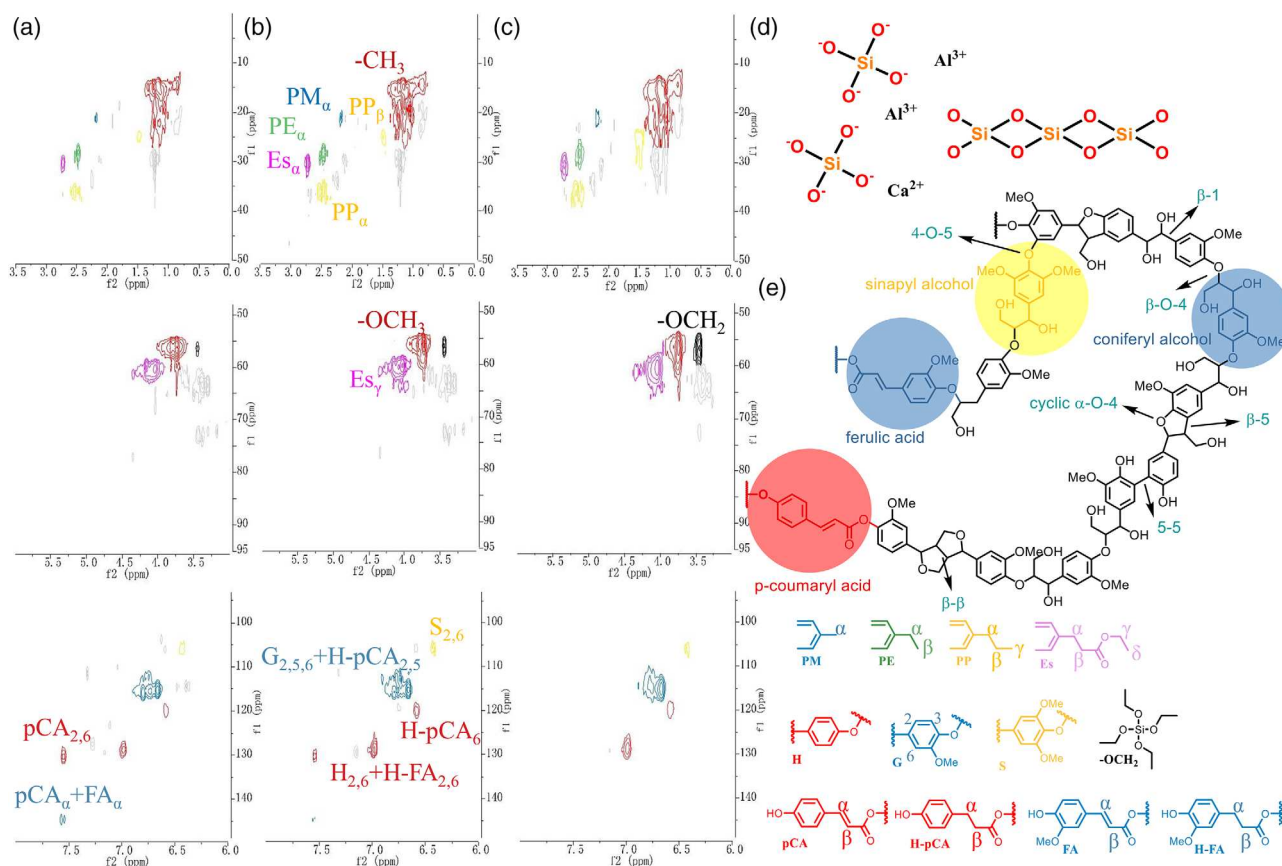


**Figure 5.** The 2D HSQC NMR spectra of liquid products obtained from CSEL depolymerization of a) 1 h, b) 4 h, and c) 8 h over Ru/SBA-15 catalyst at  $280^\circ\text{C}$  under 2 MPa H<sub>2</sub>, d) possible form of Si species in CSEL, and e) a representative of lignin fragments in CSEL.



26.6°, 27.9°, and 50.1° correspond to SiO<sub>2</sub> (PDF#46-1045) or CaAl<sub>2</sub>Si<sub>2</sub>O<sub>8</sub>·4H<sub>2</sub>O ((PDF#20-0452), and the structure of the two possible species is shown in Figure 5d, which is consistent with the large amount of Si in CSEL. The scanning electron microscopy (SEM) images of CSEL and the ash of CSEL (16.06 wt%) are shown in Figure S5, Supporting Information. The corresponding elemental mapping images are used to measure the content of Si, and the relative content of Si in ash is 31.85 wt%, which is consistent well with that in CSEL before calcination (4.94 wt%).

**NMR Characterization of the Liquid Products:** The 2D HSQC NMR spectra of the liquid products of CSEL depolymerized over Ru/SBA-15 in ethanol with 1, 4, and 8 h are shown in Figure 5. The spectra could be recognized as three regions: the aliphatic side chain region ( $\delta\text{C}/\delta\text{H}$  0–50/0–3.5 ppm), the aliphatic oxygenated side chain region ( $\delta\text{C}/\delta\text{H}$  45–95/3.0–6.0 ppm), and the aromatic bond correlation region ( $\delta\text{C}/\delta\text{H}$  95–150/6.0–8.0 ppm).<sup>[2c,16b,29]</sup> In the aliphatic side chain region, the intensity of the signals of –CH<sub>3</sub> and –OCH<sub>3</sub> shows no obvious change with different times; however, the signal that appeared at  $\delta\text{C}/\delta\text{H}$  30/2.75 and 62/4.25 ppm of ester side chains (Es<sub>α</sub> and Es<sub>γ</sub>) becomes stronger with the increase in time. The aromatic side chains of the C<sub>α</sub>–H<sub>α</sub> cross signal of para-methyl (PM<sub>α</sub>), para-ethyl (PE<sub>α</sub>), and para-propyl (PP<sub>α</sub>), are also detected with the signal of PE<sub>α</sub> slightly stronger with time, which corresponds to the large amount of ethylphenols in the product.<sup>[2c]</sup> Furthermore, the single in aliphatic oxygenated side chain region appeared at  $\delta\text{C}/\delta\text{H}$  56.4/3.44 ppm is significantly stronger with time, which might belong to siloxane. In the aromatic bond region, there has been the signals of G and hydrogenated p-coumaric/ferulic acid derivatives (H-pCA/H-FA) observed, due to the hydrogenation of the –HC=CH– over the catalyst at 280 °C. The C–H cross signals of pCA and FA units completely disappear at 8 h (Figure 3c), which implies the conversion of pCA and FA to ethylphenols via a hydrolysis–decarboxylation–hydrogenation route. Meanwhile, the C–H cross signal of S unit is extremely weak, which might be ascribed to low content of S units in corn stover.<sup>[11,16b]</sup> On the other hand, the –OCH<sub>3</sub> group might also be cleaved in this system to form EMOS.

### 3. Conclusion

For the depolymerization of industrial grade CSEL over Ru/SBA-15, a high yield of monophenol (13.91 wt%) with 61.2% selectivity to ethylphenols is obtained in the H<sub>2</sub>O/isopropanol cosolvent system, and a yield of 12.72 wt% with 55.6% ethylphenols is obtained in H<sub>2</sub>O/ethanol cosolvent. An unexpected and potentially very important aspect of these systems is the formation of significant quantities of industrially important alkoxysilanes. Similar to our previously reported formation of the valuable platform molecule LGO, these can be attributed to reaction of non-lignin materials that are present in the biomass (in this case, silicates). The organic siloxanes could be obtained at a yield as high as 61.63 wt% (representing a conversion of 61.63% of the silicates) in a system that also gives a high selectivity to H-type phenols (≈50%). Our work clearly demonstrates the complexity of industrial lignins that goes beyond the widely discussed complex and variable structure of the lignin itself but also shows

ways to exploit this through the formation of valuable chemicals and, thus, increase the potential for future multiple products, zero waste biorefineries.

### 4. Experimental Section

**Materials:** The CSEL was provided by the Institute of Process Engineering, Chinese Academy of Sciences, Beijing. Ethanol (AR) and methanol (AR) were purchased from Chengdu Kelong Chemical Co., Ltd. without further purification. Isopropanol (AR) was purchased from Chengdu Jinshan Chemical Co., Ltd. without further purification. All chemicals used for standard samples for the identification were obtained from commercial resources and used without further treatment.

The enzymatic hydrolysis lignin was obtained from bio-ethanol production using the steam-exploded-pretreated corn stover.<sup>[30]</sup> The main components of CSEL were determined according to the National Renewable Energy Laboratory (NREL) analytic methods.<sup>[31]</sup> The moisture content of CSEL was measured by drying in an oven at 105 °C overnight until constant weight was achieved. CSEL (100 mg) was treated in 72% H<sub>2</sub>SO<sub>4</sub> at 30 °C for 60 min, then diluted to 4% H<sub>2</sub>SO<sub>4</sub> by adding 28 mL deionized water, and autoclaved at 121 °C for 60 min. The hydrolysate was filtered with a porous crucible and washed with deionized water four times. The porous crucible was dried in an oven at 105 °C overnight before and after filtering the hydrolysate to weigh the acid hydrolysis solid residue. Finally, the solid residue was calcined in a crucible at 625 °C for 2 h to determine the ash content and acid insoluble lignin (AIL). The hydrolysate was analyzed by the ultra violet (UV, U-4100) and high performance liquid chromatography (HPLC, Waters-e2695) to determine the amount of acid soluble lignin (ASL) and sugar-derived products. The inorganic elements were determined by inductively coupled plasma atomic emission spectroscopy (ICP-AES) and energy-dispersive X-ray spectroscopy (EDS) mapping for Si. The main components were 62.55 wt% lignin, 9.73 wt% cellulose, 2.10 wt% hemicellulose, 16.06 wt% ash, and 5.72 wt% water. The weight percentages of C, H, O, and N are 44.52, 4.22, 49.79, and 1.47 wt%, respectively. For the inorganic elements of CSEL, Si (4.94 wt%), Al (0.42 wt%), Ca (0.26 wt%), Fe (0.62 wt%), Na (0.19 wt%), K (0.18 wt%), and Mg (0.10 wt%) account for the majority.

**Catalyst Preparation:** Ru/SBA-15 catalysts were prepared via the incipient-wetness impregnation method. Before use, SBA-15 were pre-calcined at 550 °C for 4 h and then tablet grinded to 80–120 meshes, which would facilitate the separation of catalyst from the solid residue after reaction. Typically, SBA-15 carrier was slowly poured into a desired amount of aqueous solution of RuCl<sub>3</sub>, and then shaking for 24 h at 30 °C after ultrasonically dispersed for 1 h. After heating the catalyst precursor in a water bath at 80 °C, the resulting solid was dried overnight at 80 °C, and then calcined in a muffle furnace at 400 °C (2 °C min<sup>–1</sup>) for 4 h. Before reaction, the obtained catalyst was pre-reduced in H<sub>2</sub> atmosphere with a flow rate of 40 mL min<sup>–1</sup> at 300 °C for 2 h.

**Experimental Operation and Characterization:** The depolymerization of CSEL was performed in a 100 mL Parr reactor. In a typical reaction, 0.5 g CSEL, 0.2 g Ru/SBA-15, and 50 mL solvent were added to the Parr reactor. The Parr reactor was flushed with N<sub>2</sub> for three times, and finally filled with 2 MPa H<sub>2</sub> for reaction. Then, the reactor was set to desired temperature with stirring at 400 r min<sup>–1</sup> and maintained at reaction temperature for prescribed time. Postreaction, the reactor was cooled to room temperature, and the mixture was filtered, and the solution was analyzed qualitatively and quantitatively for yield calculation.

**Characterization of Depolymerization Products:** The products of the reaction were analyzed qualitatively using GC-MS (Agilent 6820), and the quantification of the products was performed using GC equipped with a flame ionization detector (GC-FID; PERKINELMER Clarus 580). A DB-5 capillary column (30 mm × 0.25 mm × 0.25 μm) was used in both GC and GC-MS, and the flow rate of nitrogen carrier gas was 1 mL min<sup>–1</sup>, and the temperature program was set as rising with a ramp of 5 °C min<sup>–1</sup> from 50 to 250 °C and maintaining for 10 min. Injector and detector temperatures were set at 280 and 330 °C, respectively. Acetophenone was used as an



internal standard. Due to the lack of standard chemical, the relative correction factors for EMOS, TEMOS, TMOS, and TIPOS were obtained based on the effective carbon number (ECN) calculation method.<sup>[32]</sup> The yield of siloxanes was calculated by Equation (1) based on the content of Si element (4.94 wt%) in CSEL, and the yield of monophenols and the selectivity toward one specific depolymerized product were calculated by Equation (2) and (3).

$$\text{Yield of siloxane (wt\%)} = \frac{\text{Weight of Si in siloxane}}{\text{Weight of Si in CSEL}} \times 100\% \quad (1)$$

$$\text{Yield of monophenols (wt\%)} = \frac{\text{Weight of total monophenols}}{\text{Weight of lignin in CSEL}} \times 100\% \quad (2)$$

$$\begin{aligned} \text{Selectivity of specific monophenol (\%)} \\ = \frac{\text{Yield of specific monophenol}}{\text{Total yield of monophenols}} \times 100\% \end{aligned} \quad (3)$$

For the analysis of QTOF MS, the liquid product was diluted by dichloromethane (DCM) to about 100  $\mu\text{g mL}^{-1}$ . All mass spectra were acquired on an AB SCIEX QTOF X500R (AB Sciex Pte. Ltd.) with an electrospray ionization (ESI) probe and operated with spray voltage (5.5 kV), temperature (500 °C), and accumulation time (0.1 s).

For the analysis of 2D HSQC NMR, the solvent of reaction mixture (10 mL, 1/5 of the total) was removed through vacuum evaporation, and the obtained products were redissolved in 0.5 mL DMSO- $d_6$ . The 2D HSQC spectra were recorded on a Bruker AVANCE 600 MHz spectrometer, and the spectral widths were from 10 to 0 ppm and 150 to 0 ppm for  $^1\text{H}$  and  $^{13}\text{C}$  dimensions, respectively.

**Characterization of Catalyst and Materials:** Powder XRD was used to analyze the crystalline phase of the catalysts and the CSEL samples. The diffraction patterns were obtained using a Shimadzu XRD-6100 diffractometer with Cu-K $\alpha$  monochromatized radiation ( $\lambda = 1.5406 \text{ \AA}$ ) at 40 kV and 30 mA, and the scanning angle was recorded over the  $2\theta$  range of  $5^\circ$ – $80^\circ$  at a scan rate of  $5^\circ \text{ min}^{-1}$ .

$\text{N}_2$  adsorption–desorption isotherms were used to analyze the surface areas and the pore volumes, using a Micromeritics Tristar II 3020 analyzer. The samples were pretreated at 120 °C for 2 h and then evacuated at 300 °C for 2 h to remove the physically adsorbed impurities under vacuum. The surface areas were determined by the BET equation, and the pore volumes were determined by the Barrett–Joyner–Halenda (BJH) method.

XPS measurements were used to analyze the chemical state of surface species, which was carried out on an AXIS Ultra DLD (KRATOS) spectrometer with a monochromatic Al K $\alpha$  X-ray source as the excitation source. The binding energy was internally calibrated by setting the C1s peak at 284.8 eV.

ICP-AES was used to analyze the actual metal loading of the catalysts and the inorganic elements of CSEL using Thermo Elemental IRIS Advantage ER/S spectrometer (Thermo Elemental, MA, USA). The catalyst was dissolved in aqua regia, and the ash of the CSEL was dissolved in hydrochloric acid, respectively, and then diluted with deionized water before measurement.

SEM combining EDS was used to characterize the content of Si in CSEL. The samples were tested using an Apreo S (thermoscientific) combine OXFORD 80 instrument with the acceleration voltage of 20 kV. The samples were tableted before the test to obtain a relatively uniform element content of distribution.

TEM and HRTEM images were used to analyze the dispersity and crystal orientation of the supported metals. The samples were tested using a TECNAI G2-20 TWIN (FEI Co., German) instrument at an acceleration voltage of 200 kV.

## Supporting Information

Supporting Information is available from the Wiley Online Library or from the author.

## Acknowledgements

This work was financially supported by the National Natural Science Foundation of China (No. 21536007), the 111 project (No. B17030), and the Fundamental Research Funds for the Central Universities. The authors acknowledge the help of Analysis and Test Center of Sichuan University.

## Conflict of Interest

The authors declare no conflict of interest.

## Data Availability Statement

Research data are not shared.

## Keywords

depolymerization, lignin, Ru/SBA-15, siloxane, waste

Received: February 26, 2021

Revised: April 27, 2021

Published online:

- [1] a) E. M. Anderson, R. Katahira, M. Reed, M. G. Resch, E. M. Karp, G. T. Beckham, Y. Román-Leshkov, *ACS Sustainable Chem. Eng.* **2016**, 4, 6940; b) A. J. Ragauskas, G. T. Beckham, M. J. Biddy, R. Chandra, F. Chen, M. F. Davis, B. H. Davison, R. A. Dixon, P. Gilna, M. Keller, P. Langan, A. K. Naskar, J. N. Saddler, T. J. Tschaplinski, G. A. Tuskan, C. E. Wyman, *Science* **2014**, 344, 1246843; c) M. M. Abu-Omar, K. Barta, G. T. Beckham, J. Luterbacher, J. Ralph, R. Rinaldi, Y. Roman-Leshkov, J. Samec, B. Sels, F. Wang, *Energy Environ. Sci.* **2021**, 14, 262.
- [2] a) M. V. Galkin, J. S. Samec, *ChemSusChem* **2016**, 9, 1544; b) W. Schutyser, A. T. Renders, S. Van den Bosch, S.-F. Koelewijn, G. Beckham, B. F. Sels, *Chem. Soc. Rev.* **2018**, 47, 852; c) S. Van den Bosch, W. Schutyser, R. Vanholme, T. Driessen, S. F. Koelewijn, T. Renders, B. De Meester, W. J. J. Huijgen, W. Dehaen, C. M. Courtin, B. Lagrain, W. Boerjan, B. F. Sels, *Energy Environ. Sci.* **2015**, 8, 1748.
- [3] a) Z. Sun, B. Fridrich, A. de Santi, S. Elangovan, K. Barta, *Chem. Rev.* **2018**, 118, 614; b) C. Xu, R. A. Arancon, J. Labidi, R. Luque, *Chem. Soc. Rev.* **2014**, 43, 7485.
- [4] a) R. Rinaldi, R. Jastrzebski, M. T. Clough, J. Ralph, M. Kennema, P. C. Bruijninx, B. M. Weckhuysen, *Angew. Chem., Int. Ed.* **2016**, 55, 8164; b) C. Li, X. Zhao, A. Wang, G. W. Huber, T. Zhang, *Chem. Rev.* **2015**, 115, 11559.
- [5] X. Wu, N. Luo, S. Xie, H. Zhang, Q. Zhang, F. Wang, Y. Wang, *Chem. Soc. Rev.* **2020**, 49, 6198.
- [6] a) Y. Liao, S.-F. Koelewijn, G. V. D. Bossche, J. V. Aelst, S. V. D. Bosch, T. Renders, K. Navare, T. Nicolai, K. V. Aelst, M. Maesen, H. Matsushima, J. M. Thevelein, K. V. Acker, B. Lagrain, D. Verboekend, B. F. Sels, *Science* **2020**, 367, 1385; b) T. Renders, S. Van den Bosch, S. F. Koelewijn, W. Schutyser, B. F. Sels, *Energy Environ. Sci.* **2017**, 10, 1551.
- [7] J. Hu, Q. Zhang, D.-J. Lee, *Bioresour. Technol.* **2018**, 247, 1181.
- [8] H. Zhou, H. Wang, F. A. Perras, P. Naik, M. Pruski, A. D. Sadow, I. I. Slowing, *Green Chem.* **2020**, 22, 4676.
- [9] I. Haq, P. Mazumder, A. S. Kalamdhad, *Bioresour. Technol.* **2020**, 312, 123636.

- [10] T. Renders, G. Van den Bossche, T. Vangeel, K. Van Aelst, B. Sels, *Curr. Opin. Biotechnol.* **2019**, 56, 193.
- [11] X. Liu, F. P. Bouxin, J. Fan, V. L. Budarin, C. Hu, J. H. Clark, *ChemSusChem* **2020**, 13, 4296.
- [12] C. Crestini, H. Lange, M. Sette, D. S. Argyropoulos, *Green Chem.* **2017**, 19, 4104.
- [13] J.-M. Ha, K.-R. Hwang, Y.-M. Kim, J. Jae, K. H. Kim, H. W. Lee, J.-Y. Kim, Y.-K. Park, *Renewable Sustainable Energy Rev.* **2019**, 111, 422.
- [14] a) M. De bruyn, J. Fan, V. L. Budarin, D. J. Macquarrie, L. D. Gomez, R. Simister, T. J. Farmer, W. D. Raverty, S. J. McQueen-Mason, J. H. Clark, *Energy Environ. Sci.* **2016**, 9, 2571; b) R. A. Milescu, C. R. McElroy, T. J. Farmer, P. M. Williams, M. J. Walters, J. H. Clark, *Adv. Polym. Tech.* **2019**, 2019, 1.
- [15] a) S. Li, *Int. J. Electrochem. Sci.* **2019**, 11641; b) P. Chen, Q. Zhang, R. Shu, Y. Xu, L. Ma, T. Wang, *Bioresour. Technol.* **2017**, 226, 125.
- [16] a) J. Hu, S. Wu, X. Jiang, R. Xiao, *Energy Fuels* **2018**, 32, 1843; b) H. Kim, D. Padmakshan, Y. Li, J. Rencoret, R. D. Hatfield, J. Ralph, *Biomacromolecules* **2017**, 18, 4184.
- [17] T. Renders, S. Van den Bosch, T. Vangeel, T. Ennaert, S.-F. Koelewijn, G. Van den Bossche, C. M. Courtin, W. Schutyser, B. F. Sels, *ACS Sustainable Chem. Eng.* **2016**, 4, 6894.
- [18] a) Q. Fang, Z. Jiang, K. Guo, X. Liu, Z. Li, G. Li, C. Hu, *Appl. Catal., B* **2020**, 263; b) X. Liu, S. Feng, Q. Fang, Z. Jiang, C. Hu, *Mol. Catal.* **2020**, 495.
- [19] a) Z. Jiang, C. Hu, *J. Energy Chem.* **2016**, 25, 947; b) X. Zhang, Q. Zhang, J. Long, Y. Xu, T. Wang, L. Ma, Y. Li, *BioResources* **2014**, 9, 3347.
- [20] Y. Bai, K. Cui, Y. Sang, K. Wu, F. Yan, F. Mai, Z. Ma, Z. Wen, H. Chen, M. Chen, Y. Li, *Energy Fuels* **2019**, 33, 8657.
- [21] B. Jiang, J. Hu, Y. Qiao, X. Jiang, P. Lu, *Energy Fuels* **2019**, 33, 8786.
- [22] J. L. Wen, S. L. Sun, B. L. Xue, R. C. Sun, *Materials* **2013**, 6, 359.
- [23] a) S. V. Vassilev, D. Baxter, L. K. Andersen, C. G. Vassileva, *Fuel* **2010**, 89, 913; b) T. R. Miles, J. Miles, T. R. Miles, L. L. Baxter, R. W. Bryers, B. M. Jenkins, L. L. Oden, *National Renewable Energy Laboratory (NREL/TZ-2-11226-1; TP-433-8142)*, Golden, CO **1995**.
- [24] L. Li, L. Dong, D. Li, Y. Guo, X. Liu, Y. Wang, *ACS Catal.* **2020**, 10, 15197.
- [25] a) M. A. Hossain, T. K. Phung, M. S. Rahaman, S. Tulaphol, J. B. Jasinski, N. Sathitsuksanoh, *Appl. Catal., A* **2019**, 582; b) C. Zhang, C. Jia, Y. Cao, Y. Yao, S. Xie, S. Zhang, H. Lin, *Green Chem.* **2019**, 21, 1668.
- [26] K. Ooya, J. Li, K. Fukui, S. Iimura, T. Nakao, K. Ogasawara, M. Sasase, H. Abe, Y. Niwa, M. Kitano, H. Hosono, *Adv. Energy Mater.* **2020**.
- [27] S. Yang, X. Lu, H. Yao, J. Xin, J. Xu, Y. Kang, Y. Yang, G. Cai, S. Zhang, *Green Chem.* **2019**, 21, 597.
- [28] W. Fu, W. Chen, G. Qian, D. Chen, W. Yuan, X. Zhou, X. Duan, *React. Chem. Eng.* **2019**, 4, 316.
- [29] Y. Sang, K. Wu, Q. Liu, Y. Bai, H. Chen, Y. Li, *Energy Fuels* **2021**, 35, 519.
- [30] G. Wang, H. Chen, *Sep. Purif. Technol.* **2016**, 157, 93.
- [31] A. Sluiter, B. Hames, R. Ruiz, C. Scarlata, J. Sluiter, D. Templeton, D. Crocker, *Technical Report NREL/TP-510-42618*, National Renewable Energy Laboratory, Golden, CO **2010**.
- [32] S. Van den Bosch, W. Schutyser, S. F. Koelewijn, T. Renders, C. M. Courtin, B. F. Sels, *Chem. Commun.* **2015**, 51, 13158.